

1

Abstract

2

# Measurement of total hadronic differential cross sections in the LArIAT experiment

3

4

Elena Gramellini

5

2018

6

Abstract goes here. Limit 750 words.

7 **Measurement of total hadronic differential**  
8 **cross sections in the LArIAT experiment**

9 A Dissertation  
10 Presented to the Faculty of the Graduate School  
11 of  
12 Yale University  
13 in Candidacy for the Degree of  
14 Doctor of Philosophy

15 by  
16 Elena Gramellini

17 Dissertation Director: Bonnie T. Fleming

18 Date you'll receive your degree



21

*A mia mamma e mio babbo,*

22

*grazie per le radici e grazie per le ali.*

23

*To my mom and dad,*

24

*thank you for the roots and thank you for the wings.*

# Contents

25		
26	<b>Acknowledgements</b>	<b>vi</b>
27	<b>0 Total Hadronic Cross Section Measurement Methodology</b>	<b>1</b>
28	0.1 Event Selection . . . . .	2
29	0.1.1 Selection of Beamline Events . . . . .	2
30	0.1.2 Particle Identification in the Beamline . . . . .	3
31	0.1.3 TPC Selection: Halo Mitigation . . . . .	3
32	0.1.4 TPC Selection: Shower Removal . . . . .	4
33	0.2 Beamline and TPC Handshake: the Wire Chamber to TPC Match . .	5
34	0.3 The Thin Slice Method . . . . .	7
35	0.3.1 Cross Sections on Thin Target . . . . .	7
36	0.3.2 Not-so-Thin Target: Slicing the Argon . . . . .	8
37	0.3.3 Corrections to the Raw Cross Section . . . . .	10
38	0.4 Procedure testing with truth quantities . . . . .	11
39	<b>1 Preparatory Work</b>	<b>14</b>
40	1.1 Cross Section Analyses Data Set . . . . .	14
41	1.2 Construction of a Monte Carlo Simulation for LArIAT . . . . .	16
42	1.2.1 G4Beamline . . . . .	16
43	1.2.2 Data Driven MC . . . . .	20
44	1.2.3 Estimate of Energy Loss before the TPC . . . . .	21

45	1.3 Tracking Studies . . . . .	21
46	1.3.1 Study of WC to TPC Match . . . . .	21
47	1.4 Energy Calibration and Studies . . . . .	21
48	<b>2 Negative Pion Cross Section Measurement</b>	<b>23</b>
49	2.1 Raw Cross Section . . . . .	23
50	2.2 Background Subtracted Cross Section . . . . .	23
51	2.3 Efficiency Corrected Cross Section . . . . .	23
52	<b>3 Positive Kaon Cross Section Measurement</b>	<b>24</b>
53	3.1 Raw Cross Section . . . . .	24
54	<b>A Measurement of LArIAT Electric Field</b>	<b>25</b>

# Acknowledgements

*“Dunque io ringrazio tutti quanti.  
Specie la mia mamma che mi ha fatto così funky.”*  
– Articolo 31, Tanqi Funky, 1996 –

*“At last, I thank everyone.  
Especially my mom who made me so funky.”*  
– Articolo 31, Tanqi Funky, 1996 –

A lot of people are awesome, especially you, since you probably agreed to read  
this when it was a draft.

# Chapter 0

## Total Hadronic Cross Section

## Measurement Methodology

This chapter describes the general procedure employed to measure a total hadronic differential cross section in LArIAT. Albeit with small differences, both the  $(\pi^-, \text{Ar})$  and  $(K^+, \text{Ar})$  total hadronic cross section measurements rely on the same procedure described in details in the following sections. We start by selecting the particle of interest using a combination of beamline detectors and TPC information (Section ??). We then perform a handshake between the beamline information and the TPC tracking to assure the selection of the right TPC track (Section 0.2). Finally, we apply the “thin slice” method and measure the “raw” hadronic cross section (Section 0.3). A series of corrections are then evaluated to obtain the “true” cross section (Section 0.3.3).

At the end of this chapter, we show a sanity check of the methodology against MC truth information (Section 0.4).



## 0.1 Event Selection

The measurement of the  $(\pi^-, \text{Ar})$  and  $(K^+, \text{Ar})$  total hadronic cross section in LArIAT starts by selecting the pool of pion or kaon candidates and measuring their momentum. This is done through the series of selections on beamline and TPC information described in the next sections. The summary of the event selection in data is reported in Table 1.

### 0.1.1 Selection of Beamline Events

As shown in equation 5, we leverage the beamline particle identification and momentum measurement before entering the TPC as in input to evaluate the kinetic energy for the hadrons used in the cross sections measurements. Thus, we select the LArIAT data to keep only events whose wire chamber and time of flight information is registered (line 2 in in Table 1). Additionally, we perform a check of the plausibility of the trajectory inside the beamline detectors: given the position of the hits in the four wire chambers, we make sure the particle's trajectory does not cross any impenetrable material such as the collimator and the magnets steel (line 3 in in Table 1).

	Run-II Negative Polarity	Run-II Positive Polarity
Events Reconstructed in Beamline	158396	260810
Events with Plausible Trajectory	147468	240954
Beamline $\pi^-/\mu^-/e^-$ Candidate	138481	N.A.
Beamline $K^+$ Candidate	N.A	2837
Events Surviving Pile Up Filter	108929	2389
Events with WC2TPC Match	41757	1081
Events Surviving Shower Filter	40841	N.A.
Available Events For Cross Section	40841	1081

Table 1: Number of data events for Run-II Negative and Positive polarity

### 94 0.1.2 Particle Identification in the Beamline

95 In data, the main tool to establish the identity of the hadron of interest is the LArIAT  
 96 tertiary beamline, in its function of mass spectrometer. We combine the measurement  
 97 of the time of flight,  $TOF$ , and the beamline momentum,  $p_{Beam}$ , to reconstruct the  
 98 invariant mass of the particles in the beamline,  $m_{Beam}$ , as follows

$$m_{Beam} = \frac{p_{Beam}}{c} \sqrt{\left(\frac{TOF * c}{l}\right)^2 - 1}, \quad (1)$$

99 where  $c$  is the speed of light and  $l$  is the length of the particle's trajectory between  
 100 the time of flight paddels.

101 Figure 1 shows the mass distribution for the Run II negative polarity runs on the  
 102 left and positive polarity runs on the right. We perform the classification of events  
 103 into the different samples as follows:

- 104 •  $\pi/\mu/e$ : mass < 350 MeV
- 105 • kaon: 350 MeV < mass < 650 MeV
- 106 • proton: 650 MeV < mass < 3000 MeV.

107 Lines 4 and 5 in in Table 1 show the number of negative  $\pi/\mu/e$  and positive  $K$   
 108 candidates which pass the mass selection for LArIAT Run-II data.

### 109 0.1.3 TPC Selection: Halo Mitigation

110 The secondary beam impinging on LArIAT secondary target produces a plethora of  
 111 particles which propagates downstream. The presence of upstream and downstream  
 112 collimators greatly abates the number of particles tracing down the LArIAT tertiary  
 113 beamline. However, it is possible that more than one particle sneaks into the LArTPC  
 114 during its readout time: the TPC readout is triggered by the particle firing the

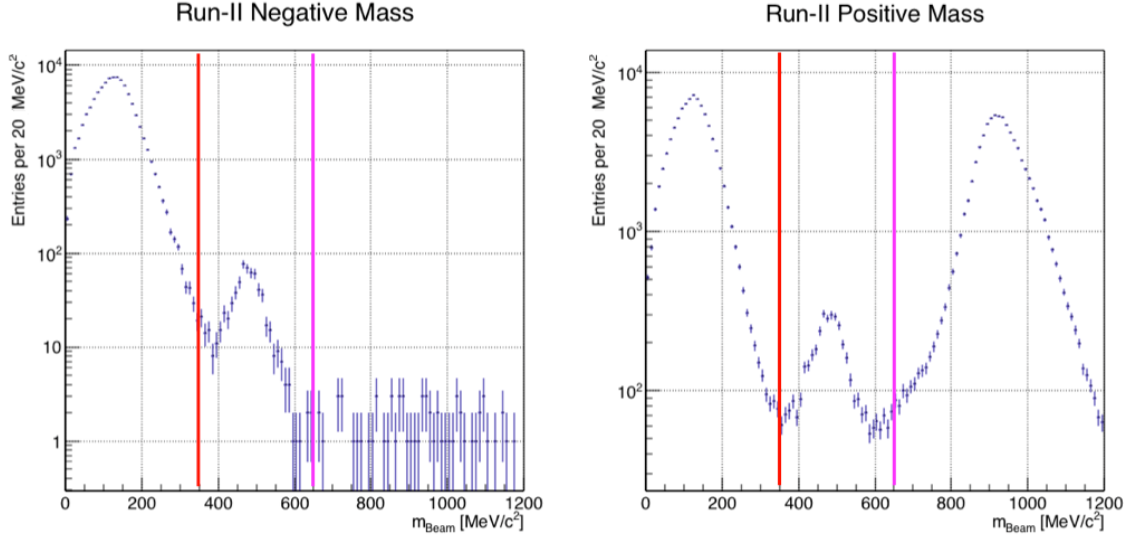


Figure 1: Distribution of the beamline mass as calculated according to equation 1 for the Run-II events reconstructed in the beamline, negative polarity runs on the left and positive polarity runs on the right. The classification of the events into  $\pi^\pm/\mu^\pm/e^\pm$ ,  $K^\pm$ , or (anti)proton is based on these distributions, whose selection cut are represented by the vertical colored lines.

beamline detectors, but particles from the beam halo might be present in the TPC at the same time. We call “pile up” the additional traces in the TPC. We adjusted the primary beam intensity between LArIAT Run I and Run II to reduce the presence of events with high pile up particles in the data sample. For the cross section analyses, we remove events with more than 4 tracks in the first 14 cm upstream portion of the TPC from the sample (line 6 in in Table 1).

#### 0.1.4 TPC Selection: Shower Removal

In the case of the  $(\pi^-, \text{Ar})$  cross section, the resolution of beamline mass spectrometer is not sufficient to select a beam of pure pions. In fact, muons and electrons survive the selection on the beamline mass. It is important to notice that the composition of the negative polarity beam is mostly pions, as will be discussed in section 1.2.1. Anyhow, we devise a selection on the TPC information to mitigate the presence of

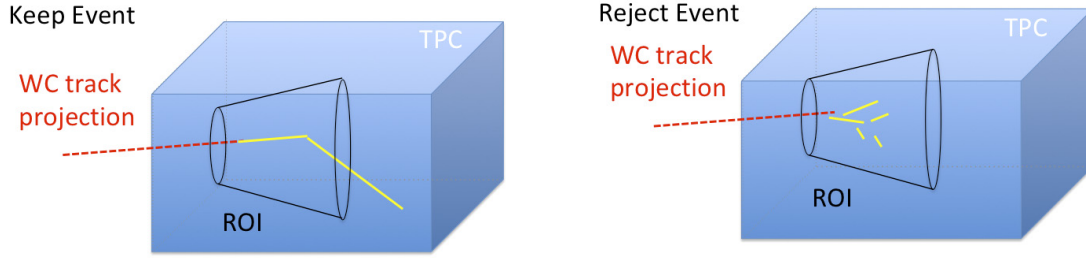


Figure 2: Visual rendering of the shower filter. The ROI is a cut cone, with a small radius of 4 cm, a big radius of 10 cm and an height of 42 cm (corresponding to 3 radiation lengths for electrons in Argon).

127 electrons in the sample used for the pion cross section. The selection relies on the  
 128 different topologies of a pion and an electron event in the argon: while the former  
 129 will trace a track inside the TPC active volume, the latter will tend to “shower”, i.e.  
 130 interact with the medium, producing bremsstrahlung photons which pair convert into  
 131 several short tracks. In order to remove the shower topology, we create a region of  
 132 interest (ROI) around the TPC track corresponding to the beamline particle (more  
 133 details on this in the next section). We look for short tracks contained in the ROI,  
 134 as depicted in figure 4: if more then 5 tracks shorter than 10 cm are in the ROI,  
 135 we reject the event. Line 8 in in Table 1) shows the number of events surviving this  
 136 selection.

## 137 **0.2 Beamline and TPC Handshake: the Wire Cham-** 138 **ber to TPC Match**

139 For each event passing the selection on its beamline information, we need to identify  
 140 the track inside the TPC corresponding to the particle which triggered the beamline  
 141 detectors, a procedure we refer to as “WC to TPC match” (WC2TPC for short).  
 142 In general, the TPC tracking algorithm will reconstruct more than one track in the  
 143 event, partially due to the fact that hadrons interact in the chamber and partially

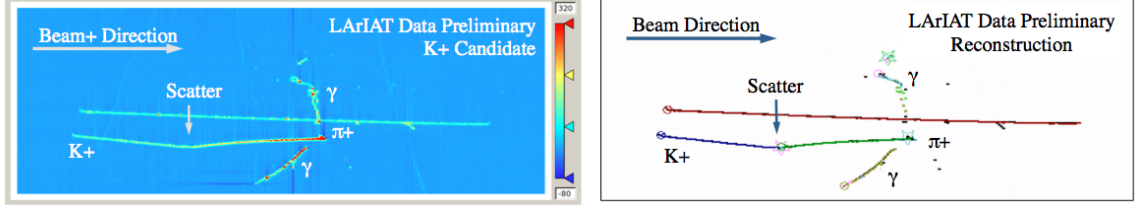


Figure 3: Kaon candidate event: on the right, event display showing raw quantities; on the left, event display showing reconstructed tracks. In the reconstructed event display, different colors represent different track objects. A kink is visible in the kaon ionization, signature of a hadronic interaction: the tracking correctly stops at the kink position and two tracks are formed. An additional pile-up track is so present in the event (top track).

144 because of pile up particles during the triggered TPC readout time, as shown in  
 145 figure 3.

146 We attempt to uniquely match one wire chamber track to one and only one re-  
 147 constructed TPC track. In order to determine if the presence of a match, we apply  
 148 a geometrical selection on the relative the position of the wire chamber and TPC  
 149 tracks. We start by considering only TPC tracks whose first point is in the first 2  
 150 cm upstream portion of the TPC for the match. We project the wire chamber track  
 151 to the TPC front face where we define the coordinates of the projected point as  $x_{FF}$   
 152 and  $y_{FF}$ . For each considered TPC track, we define  $\Delta X$  as the difference between  
 153 the  $x$  position of the most upstream point of the TPC track and  $x_{FF}$ .  $\Delta Y$  is defined  
 154 analogously. We define the radius difference,  $\Delta R$ , as  $\Delta R = \sqrt{\Delta X^2 + \Delta Y^2}$ . We de-  
 155 fine as  $\alpha$  the angle between the incident WC track and the TPC track in the plane  
 156 that contains them. If  $\Delta R < 4$  cm,  $\alpha < 8^\circ$ , a match between WC-track and TPC  
 157 reconstructed track is found. We describe how we determine the value for the radius  
 158 and angular selection in sec 1.3.1. In MC, we mimic the matching between the WC  
 159 and the TPC track by constructing a fake WC track using truth information at wire  
 160 chamber four. We then apply the same WC to TPC matching algorithm as in data.  
 161 We discard events with multiple WC2TPC matches. We use only those TPC tracks  
 162 that are matched to WC tracks in the cross section calculation.

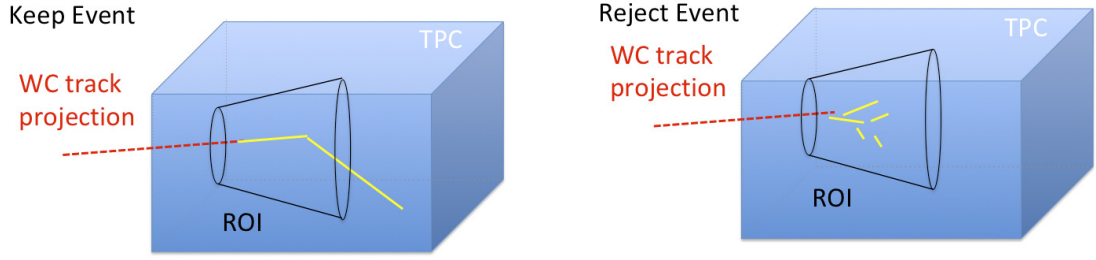


Figure 4: Visual rendering of the wire chamber to TPC match.

## 0.3 The Thin Slice Method

Once we have selected the pool of hadron candidates and we have identified the TPC track corresponding to the beamline event, we apply the thin slice method to measure the cross section, as the following sections describe.

### 0.3.1 Cross Sections on Thin Target

Cross section measurements on a thin target have been the bread and butter of nuclear and particle experimentalists since the Geiger-Marsden experiments [?]. At their core, these types of experiments consist in shooting a beam of particles with a known flux on a thin target and recording the outgoing flux.

In general, the target is not a single particle, but rather a slab of material containing many diffusion centers. The so-called “thin target” approximation assumes that the target centers are uniformly distributed in the material and that the target is thin compared to the projectile interaction length,  $WC2TPC$  so that no center of interaction sits in front of another. In this approximation, the ratio between the number of particles interacting in the target  $N_{Interacting}$  and number of incident particles  $N_{Incident}$  determines the interaction probability  $P_{Interacting}$ , which is the complementary to one of the survival probability  $P_{Survival}$ . Equation 2

$$P_{Survival} = 1 - P_{Interacting} = 1 - \frac{N_{Interacting}}{N_{Incident}} = e^{-\sigma_{TOT}n\delta X} \quad (2)$$

describes the probability for a particle to survive the thin target. This formula relates the total cross section  $\sigma_{TOT}$ , the density of the target centers  $n$  and the thickness of the target along the incident hadron direction  $\delta X$ , to the interaction probability<sup>1</sup>. If the target is thin compared to the interaction length of the process considered, we can Taylor expand the exponential function in equation 2 and find a simple proportionality relationship between the number of incident and interacting particles, and the cross section, as shown in equation 3:

$$1 - \frac{N_{Interacting}}{N_{Incident}} = 1 - \sigma_{TOT} n \delta X + O(\delta X^2). \quad (3)$$

Solving for the cross section, we find:

$$\sigma_{TOT} = \frac{1}{n \delta X} \frac{N_{Interacting}}{N_{Incident}}. \quad (4)$$

### 0.3.2 Not-so-Thin Target: Slicing the Argon

The interaction length of pions and kaons in argon is expected to be of the order of 50 cm for pions and 100 cm for kaons. Thus, the LArIAT TPC, with its 90 cm of length, is not a thin target. However, the fine-grained tracking of the LArIAT LArTPC allows us to treat the argon volume as a sequence of many adjacent thin targets.

As described in Chapter ??, LArIAT wire planes consist of 240 wires each. The wires are oriented at +/- 60° from the vertical direction at 4 mm spacing, while the beam direction is oriented 3 degrees off the  $z$  axis in the  $XZ$  plane. The wires collect signals proportional to the energy loss of the hadron along its path in a  $\delta X = 4 \text{ mm} / \sin(60^\circ) \approx 4.7 \text{ mm}$  slab of liquid argon. Thus, one can think to slice the TPC

---

1. The scattering center density in the target,  $n$ , relates to the argon density  $\rho$ , the Avogadro number  $N_A$  and the argon molar mass  $m_A$  as  $n = \frac{\rho N_A}{m_A}$ .

199 into many thin targets of  $\delta X = 4.7$  mm thickness along the direction of the incident  
 200 particle, making a measurement at each wire along the path.

201 Considering each slice  $j$  a “thin target”, we can apply the cross section calculation  
 202 from Equation 4 iteratively, evaluating the kinetic energy of the hadron as it enters  
 203 each slice,  $E_j^{kin}$ . For each WC2TPC matched particle, the energy of the hadron  
 204 entering the TPC is known thanks to the momentum and mass determination by the  
 205 tertiary beamline,

$$E_{FrontFace}^{kin} = \sqrt{p_{Beam}^2 - m_{Beam}^2} - m_{Beam} - E_{loss}, \quad (5)$$

206 where  $E_{loss}$  is a correction for the energy loss in the dead material between the  
 207 beamline and the TPC front face. The energy of the hadron at each slab is determined  
 208 by subtracting the energy released by the particle in the previous slabs. For example,  
 209 at the  $j^{th}$  point of a track, the kinetic energy will be

$$E_j^{kin} = E_{FrontFace}^{kin} - \sum_{i < j} \Delta E_i, \quad (6)$$

210 where  $\Delta E_i$  is the energy deposited at each argon slice before the  $j^{th}$  point as measured  
 211 by the calorimetry associated with the tracking.

212 If the particle enters a slice, it contributes to  $N_{Incident}(E^{kin})$  in the energy bin  
 213 corresponding to its kinetic energy in that slice. If it interacts in the slice, it then  
 214 also contributes to  $N_{Interacting}(E^{kin})$  in the appropriate energy bin. The cross section  
 215 as a function of kinetic energy,  $\sigma_{TOT}(E^{kin})$  will then be proportional to the ratio  
 216  $\frac{N_{Interacting}(E^{kin})}{N_{Incident}(E^{kin})}$ .

217 The statistical uncertainty for each energy bin is calculated by error propagation  
 218 from the statistical uncertainty on  $N_{Incident}$  and  $N_{Interacting}$ . Since the number of  
 219 incident hadrons in each energy bin is given by a simple counting, we assume that  
 220  $N_{Incident}$  is distributed as a poissonian with mean and  $\sigma^2$  equal to  $N_{Incident}$  in each



bin. On the other hand,  $N_{Interacting}$  follows a binomial distribution: a particle in a given energy bin might or might not interact. The square of the variance for the binomial is given by

$$\sigma^2 = \mathcal{N} P_{Interacting} (1 - P_{Interacting}); \quad (7)$$

since the interaction probability  $P_{Interacting}$  is  $\frac{N_{Interacting}}{N_{Incident}}$  and the number of tries  $\mathcal{N}$  is  $N_{Incident}$ , equation 7 translates into

$$\sigma^2 = N_{Incident} \frac{N_{Interacting}}{N_{Incident}} \left(1 - \frac{N_{Interacting}}{N_{Incident}}\right) = N_{Interacting} \left(1 - \frac{N_{Interacting}}{N_{Incident}}\right). \quad (8)$$

$N_{Incident}$  and  $N_{Interacting}$  are not independent. The uncertainty on the cross section is thus calculated as

$$\delta\sigma_{tot}(E) = \sigma_{tot}(E) \left( \frac{\delta N_{Interacting}}{N_{Interacting}} + \frac{\delta N_{Incident}}{N_{Incident}} \right) \quad (9)$$

where:

$$\delta N_{Incident} = \sqrt{N_{Incident}} \quad (10)$$

$$\delta N_{Interacting} = \sqrt{N_{Interacting} \left(1 - \frac{N_{Interacting}}{N_{Incident}}\right)}. \quad (11)$$

### 0.3.3 Corrections to the Raw Cross Section

Equation 4 is a prescription for measuring the cross section in case of a pure beam of the hadron of interest and 100% efficiency in the determination of the interaction point. For example, if LArIAT had a beam of pure pions and were 100% efficient in determining the interaction point within the TPC, the pion cross section in each energy bin would be given by

$$\sigma^{\pi^-}(E_i) = \frac{1}{n\delta X} \frac{N_{Interacting}^{\pi^-}(E_i)}{N_{Incident}^{\pi^-}(E_i)}. \quad (12)$$

Unfortunately, this is not the case. In fact, the selection used to isolate pions in the LArIAT beam allows for the presence of some muons and electrons as background. Also, the LArIAT TPC is not 100% efficient in determining the interaction point. Therefore we need to apply two corrections evaluated on the MC in order to extract the cross section from LArIAT data: the background subtraction and the efficiency correction. Still using the pion case as example, we estimate the pion cross section in each energy bin changing Equation 12 into

$$\sigma^{\pi^-}(E_i) = \frac{1}{n\delta X} \frac{N_{\text{Interacting}}^{\pi^-}(E_i)}{N_{\text{Incident}}^{\pi^-}(E_i)} = \frac{1}{n\delta X} \frac{\epsilon_i^{\text{inc}}[N_{\text{Interacting}}^{\text{TOT}}(E_i) - B_{\text{Interacting}}(E_i)]}{\epsilon_i^{\text{int}}[N_{\text{Incident}}^{\text{TOT}}(E_i) - B_{\text{Incident}}(E_i)]}, \quad (13)$$

where  $N_{\text{Interacting}}^{\text{TOT}}(E_i)$  and  $N_{\text{Incident}}^{\text{TOT}}(E_i)$  is the measured content of the interacting and incident histograms for events that pass the event selection,  $B_{\text{interacting}}(E_i)$  and  $B_{\text{Incident}}(E_i)$  represent the contributions from beamline background, and  $\epsilon_i^{\text{int}}$  and  $\epsilon_i^{\text{inc}}$  are the efficiency corrections for said histograms.

As we will show in section ??, the background subtraction for the interacting and incident histograms can be translated into a corresponding corrections  $C_{\text{Interacting}}^{\pi MC}(E_i)$  and  $C_{\text{Incident}}^{\pi MC}(E_i)$  and the cross section re-written as follows

$$\sigma^{\pi^-}(E_i) = \frac{1}{n\delta X} \frac{\epsilon_i^{\text{inc}} N_{\text{Interacting}}^{\text{TOT}}(E_i) C_{\text{Interacting}}^{\pi MC}(E_i)}{\epsilon_i^{\text{int}} N_{\text{Incident}}^{\text{TOT}}(E_i) C_{\text{Incident}}^{\pi MC}(E_i)}. \quad (14)$$

## 0.4 Procedure testing with truth quantities

The  $(\pi^-, \text{Ar})$  and  $(K^+, \text{Ar})$  total hadronic cross section implemented in Geant4 can be used as a tool to validate the measurement methodology. We describe here a closure test done on Monte Carlo to prove that the methodology of slicing the TPC retrieves the underlying cross section distribution implemented in Geant4 within the statistical uncertainty.

For pions in the considered energy range, **the Geant4 inelastic model adopted to**

256 is “BertiniCascade”, while the elastic model “hElasticLHEP”. For kaons, the Geant4  
257 inelastic model adopted to is “BertiniCascade”, while the elastic model “hElasti-  
258 cLHEP”.

259 For the validation test, we fire about a sample of pions and a sample of kaons  
260 inside the LArIAT TPC active volume using the Data Driven Monte Carlo (see section  
261 1.2.2). We apply the thin-sliced method using only true quantities to calculate the  
262 hadron kinetic energy at each slab in order to decouple reconstruction effects from  
263 issues with the methodology. For each slab of 4.7 mm length along the path of the  
264 hadron, we integrate the true energy deposition as given by the Geant4 transportation  
265 model. Then, we recursively subtracted it from the hadron kinetic energy at the TPC  
266 front face to evaluate the kinetic energy at each slab until the true interaction point is  
267 reached. Since the MC is a pure beam of the hadron of interest and truth information  
268 is used to retrieve the interaction point, no correction is applied. Doing so, we obtain  
269 the true interacting and incident distributions for the considered hadron and we obtain  
270 the true MC cross section as a function of the hadron true kinetic energy.

271 Figure 5 shows the total hadronic cross section for argon implemented in Geant4  
272 10.01.p3 (solid lines) overlaid with the true MC cross section as obtained with the  
273 sliced TPC method (markers) for pions on the left and kaons on the right; the total  
274 cross section is shown in green, the elastic cross section in blue and the inelastic  
275 cross section in red. The nice agreement with the Geant4 distribution and the cross  
276 section obtained with the sliced TPC method gives us confidence in the validity of  
277 the methodology.

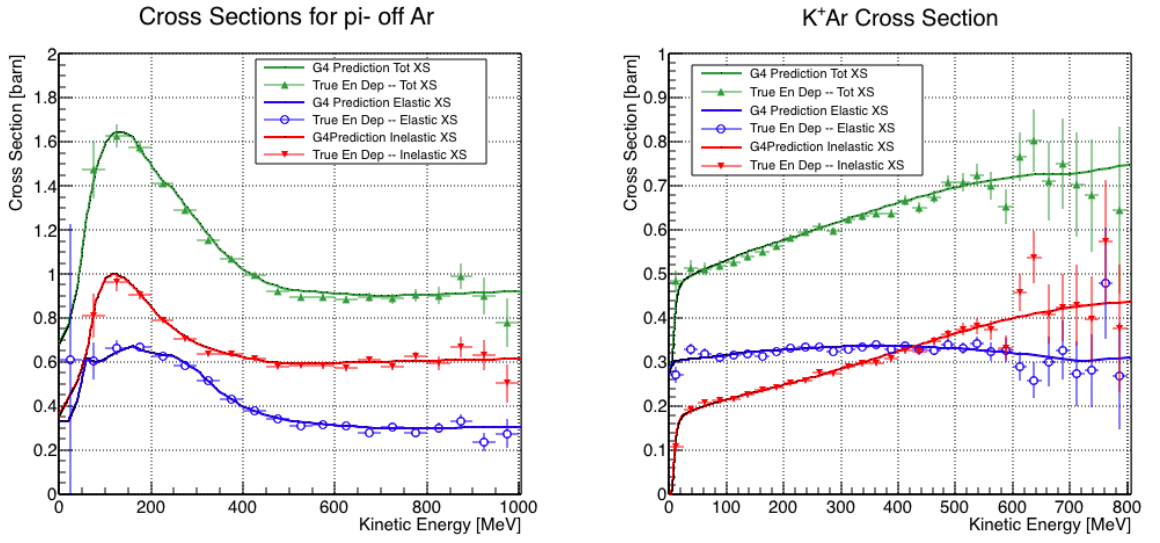


Figure 5: Hadronic cross sections for  $(\pi^-, \text{Ar})$  on the left and  $(K^+, \text{Ar})$  on the right as implemented in Geant4 10.01.p3 (solid lines) overlaid the true MC cross section as obtained with the sliced TPC method (markers). The total cross section is shown in green, the elastic cross section in blue and the inelastic cross section in red.

# Chapter 1

## Preparatory Work

This chapter describes the preparatory work done on the the data and Monte Carlo samples used for the cross section analyses. This entails the choice of the data set and the production of the information needed to construct the Monte Carlo Simulation (section 1.1), the construction and use of said Monte Carlo simulation (section 1.2), the study and optimization of the tracking in the TPC for the cross section analyses (section 1.3), the calibration of the calorimetry response and related energy studies (section 1.4).

### 1.1 Cross Section Analyses Data Set

We choose LArIAT Run-II as the data period for the  $(\pi^-, \text{Ar})$  and  $(K^+, \text{Ar})$  total hadronic cross section analyses. Data taking for the this period started on 03/15/2016 and ended on 07/31/2016. Since we are interested in beamline and TPC information, we ask basic requirements on the operational status of the time of fight, wire chambers and TPC to form the good run list for this period, which we informally call “lovely runs”.

The subset of lovely runs chosen for the  $(\pi^-, \text{Ar})$  total hadronic cross section analysis includes only the -60A and -100A magnet configurations in negative polarity,

even if LArIAT explored several other beamline configurations during Run-II. The -60A and -100A combined data set accounts for approximately 90% of the total Run-II negative polarity runs. Since the production of beamline Monte Carlo depends on the wanted beamline configuration, the choice of only two beamline settings limits the need for beamline MC production.

Similarly, the subset of lovely runs chosen for the  $(K^+, \text{Ar})$  total hadronic cross section analysis includes only the +60A and +100A magnet configurations in positive polarity. It should be noted that kaons are extremely rare in the +60A sample, thus the data sample for the  $(K^+, \text{Ar})$  cross section after the mass selection is about 90% +100A runs, as shown in Table 1.1.

For the first measurements in LArIAT that uses both beamline and TPC information, we choose strict requirements on the reconstruction of the WC tracks, the so-called “Picky Track” sample (see ??). This choice presents two advantages: the uncertainty on the momentum reconstruction for the “Picky Tracks” sample is smaller compared to the “High Yield” sample, and the comparison with the beamline MC results is straightforward. A possible future update and cross check of these analysis would be the use of the High Yield sample, where the statistics is about three times higher.

The breakdown of beamline events as a function of the magnets settings is shown in Table 1.1. The choice of the data sets determines the production of beamline MC and serves as basis for the production of Data Driven MC, as shown in the next sections.

	I = 60 A	I = 100 A	Total
Data Events after $\pi/\mu/e$ Mass Selection	67068	71413	138481
Data Events after $K$ Mass Selection	274	2563	2837

Table 1.1: Number of data events which fit the  $\pi/\mu/e$  or  $K$  mass hypothesis as a function of magnet settings.

## 1.2 Construction of a Monte Carlo Simulation for LArIAT

For the simulation of LArIAT events and their particle make up, we use a combination of two MC generators: the G4Beamline Monte Carlo and the Data Driven single particle Monte Carlo (DDMC). We use the G4Beamline MC to simulate the particle transportation in the beamline and calculate the particle composition of the beam just after the fourth Wire Chamber (WC4). In order to simulate the beamline particles after WC4 and in the TPC, we use the DDMC.

### 1.2.1 G4Beamline

G4Beamline simulates the beam collision with the LArIAT secondary target, the energy deposited by the particles in the LArIAT beamline detectors, and the action of the LArIAT magnets, effectively accounting for particle transportation through the beam line from the LArIAT target until “Big Disk”, a fictional, void detector located just before the LArIAT cryostat. At the moment of this writing, G4Beamline does not simulated the responses of the beam line detectors. It is possible to interrogate the truth level information of the simulated particles in several points of the geometry. In order to ease the handshake between G4Beamline and the DDMC, we ask for the beam composition just after WC4. Since LArIAT data are taken under different beam conditions, we need to simulate separately the beam composition according to the magnets’ settings and the secondary beam intensity with G4Beamline. For the pion cross section analysis the relevant beam conditions are secondary beam energy of 64 GeV, negative polarity magnet with current of 100 A and 60 A. For the kaon cross section analysis the relevant beam conditions is a secondary beam energy of 64 GeV, positive polarity magnet with current of 100 A.

	I = -60 A	I = -100 A
G4Pions	68.8 %	87.4 %
G4Muons	4.6 %	3.7 %
G4Electrons	26.6 %	8.9 %

Table 1.2: Simulated beamline composition per magnet settings

## 342 Beam Composition for Negative Pion Cross Section

343 Even if pions are by far the biggest beam component in negative polarity runs, the  
344 LArIAT tertiary beam is not a pure pion beam. While useful to discriminate between  
345 pions, kaons, and protons, the beamline detectors are not sensitive enough to discrim-  
346 inate among the lighter particles in the beam: electrons, muons and pions fall under  
347 the same mass hypothesis. Thus, we need to assess the contamination from beamline  
348 particles other than pions in the event selections used for the pion cross section analy-  
349 sis and correct for its effects. The first step of this process is assessing the percentage  
350 of electrons and muons in the  $\pi/\mu/e$  beamline candidates via the G4Beamline MC.  
351 The full treatment of the beamline contamination in the pion cross section calculation  
352 is described in section 2.2. Since the beamline composition is a function of the magnet  
353 settings, we simulate separately events for magnet current of -60A and -100A. Figure  
354 1.1 shows the momentum predictions from G4Beamline overlaid with data for the  
355 60A runs (left) and for the 100A runs (right). The predictions for electrons, muons  
356 and pions have been staggered and their sum is area normalized to data. Albeit not  
357 perfect, these plots show a reasonable agreement between the momentum shapes in  
358 data and MC. We attribute the difference in shape to the lack of simulation of the  
359 WC efficiency in the MC which is momentum dependent and leads to enhance the  
360 number events in the center of the momentum distribution.

361 Table 1.2 shows the beam composition per magnet setting after the mass selection  
362 according to the G4Beamline simulation.



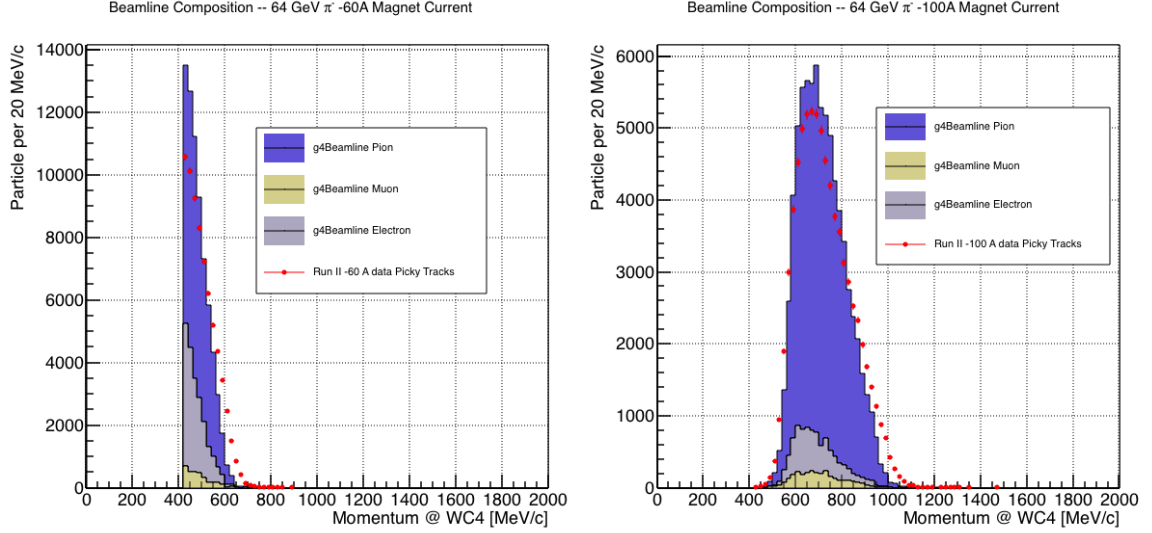


Figure 1.1: Beam composition for the -60A runs (left) and -100A runs (right). The solid blue plot represents the simulated pion content, the yellow plot represents the simulated muon content and the grey plot represents the simulated electron content. The plots are area normalized to the number of data events, shown in red.

### 363 Beam Composition for Positive Kaon Cross Section

364 In the positive polarity runs, the tertiary beam composition is mainly pions and pro-  
 365 tons. The left side of Figure 1.2 shows the predictions for the momentum spectra  
 366 for the 100A positive runs according to G4Beamline (solid colors) overlaid with data  
 367 (black points). Since the LArIAT beamline detectors can discriminate between kaons  
 368 and other particles, we do not rely on the G4Beamline simulation to estimate the  
 369 beamline contamination in the pool of kaon candidates (as in the case of the pion  
 370 cross section), but rather we use a data drive approach. The basic idea of this data  
 371 driven approach is to estimate the bleed over from high and low mass peaks under the  
 372 kaon peak by fitting the tails of the  $\pi/\mu/e$  and proton mass distributions, as shown  
 373 in Figure 1.2 right side. Since the shape of the tails is unknown, the estimate is done  
 374 multiple times varying the range and shape for reasonable functions. For example, to  
 375 estimate the proton content under the kaon peak, we start by fitting the left tail of  
 376 the proton mass distribution with a gaussian function between  $650 \text{ MeV}/c^2$  and  $750$

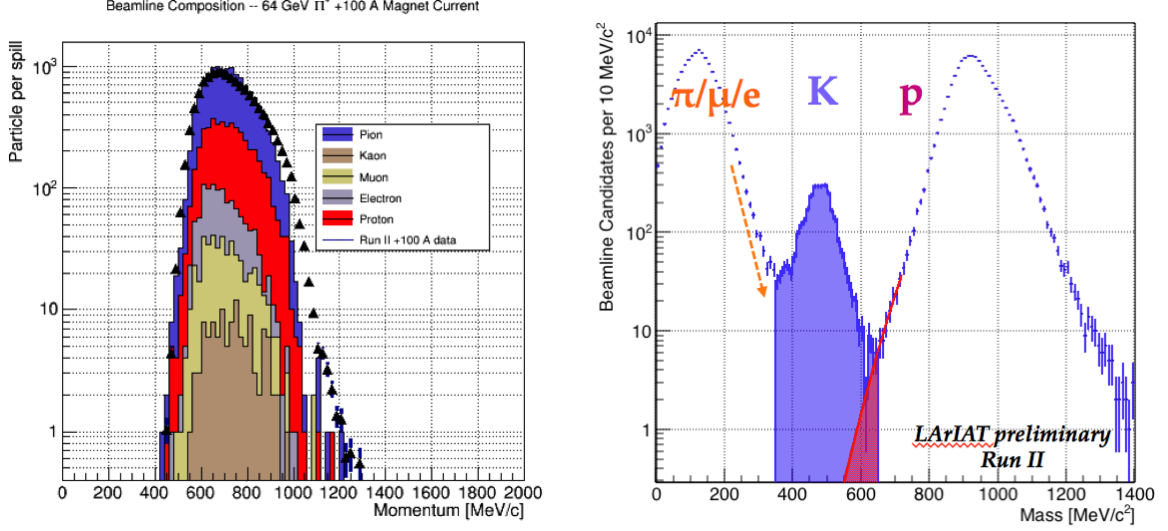


Figure 1.2: *Left*. Beam composition for the +100A runs after WC4 (no mass selection applied). The solid blue plot represents the simulated pion content, the yellow plot represents the simulated muon content and the grey plot represents the simulated positron content, the red the proton content and the mustard the kaon content. The plots are area normalized to the number of data events, shown in black. *Right*. Mass distribution for the Run-II positive runs, where the area under the kaon mass peak is highlighted in purple. The area under the extension of a possible fit for the proton tail is highlighted in red.

377  $MeV/c^2$ . We extend the fit function under the kaon peak and integrate the between  
378  $350-650 MeV/c^2$ . We integrate the mass histogram in the same range and calculate  
379 the proton contamination as the ratio between the two integrals. We repeat this pro-  
380 cedure for several fit shapes (gaussian, linear and exponential functions are used) and  
381 tail ranges. Finally, we calculate the contamination as the weighted average of single  
382 estimates, where the weights are calculated to be the  $1/\chi^2$  of the tail fits. The pro-  
383 cedure is repeated for lighter particles mass peak independently. With 12 iterations  
384 of this method we find a proton contamination of  $0.2 \pm 0.5 \%$  and a contamination  
385 from the lighter particles of  $5 \pm 2 \%$ .

### 1.2.2 Data Driven MC

The Data Driven single particle Monte Carlo (DDMC) is a single particle gun which simulates the particle transportation from WC4 into the TPC leveraging on the beam-line data information. The DDMC uses the data momentum and position at WC4 to derive the event generation: a general sketch of the DDMC workflow is shown in Figure 1.3.

When producing a DDMC sample, beam line data from a particular running period and/or running condition are selected first. For example, data for the negative 60A runs and for the negative 100A runs inform the event generation stage of two different DDMC samples. Figure 1.4 schematically shows the data quantities of interest leveraged from data: the momentum ( $P_x, P_y, P_z$ ) and position ( $X, Y$ ) at WC4. For each data event, we obtain the particle position ( $X, Y$ ) at WC4 directly from the data measurement; we calculate the components of the momentum using the beam-line measurement of the momentum magnitude in conjunction with the hits on WC3 and WC4 to determine the direction of the momentum vector, as described in section ???. The momentum and position of the selected data

The momentum and position of the selected data form a 5-dimensional tuple, which we sample thousand of times through a 5-dimensional hit-or-miss sampling procedure to generate the MC events. This produces MC  $P_x, P_y, P_z, X, Y$  distributions with the same momentum and position distributions as data, with the additional benefit of accounting for the correlations between the considered variables. A LArSoft simulation module then launches single particle MC from  $z = -100$  cm (the location of the WC4) using the sampled momentum and position distributions as a template. As an example, the results of the DDMC generation compared to data for the pion 60A sample are shown in figure ??; as expected, MC and data agree within the statistical uncertainty by construction. Using this technique ensures the MC and data particles have very similar momentum, position and angular distributions at WC4 and allow

413 us to us the MC sample in several occasions, for example to calibrate the energy loss  
 414 upstream of the TPC (see Section ??) or to study the tracking and the calorimetric  
 415 performance (sections 1.3 and 1.4). A small caveat is in order here: the DDMC is a  
 416 single particle Monte Carlo, which means that the beam pile-up is not simulated.  
 417 Three sample of **NUMBERS** pions, muons and electrons, as well as a sample of  
 418 **NUMBERS** kaons have been generated with the DDMC and are used for the MC  
 419 cross section study.

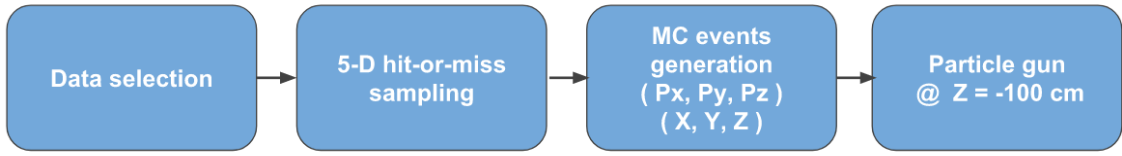


Figure 1.3: Workflow for Data Driven single particle Monte Carlo production.

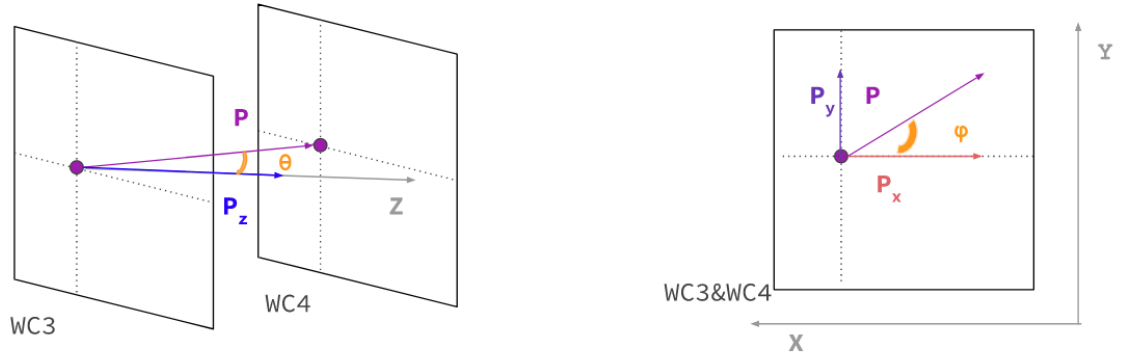


Figure 1.4: Scheme of the quantities of interest for the DDMC event generation:  $P_x, P_y, P_z, X, Y$  at WC4.

## Momentum Z Component

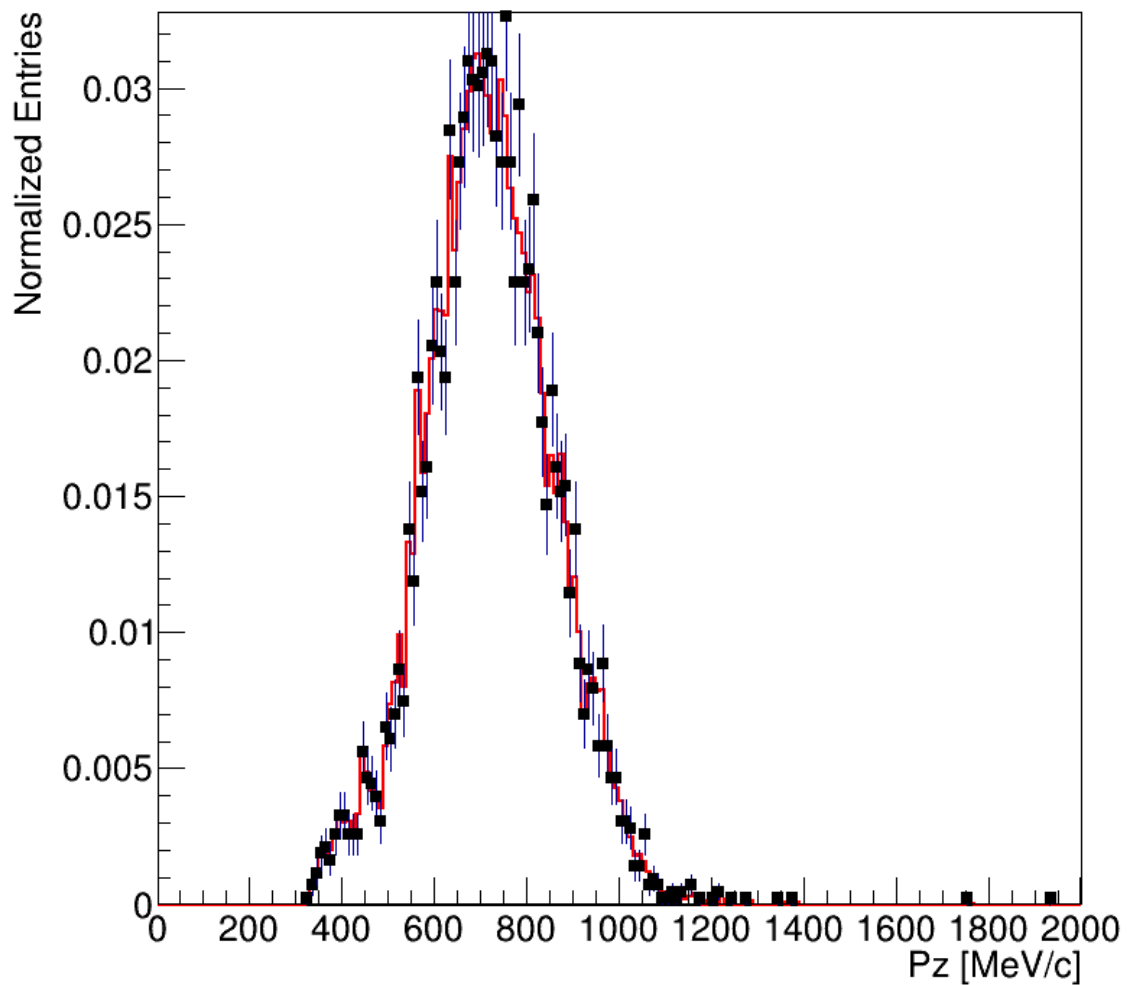


Figure 1.5: Comparison between generated quantities and data distributions for the 60A pion sample: Z component of the momentum (top left), X position at Wire Chamber 4 (top right), Y position at Wire Chamber 4 (bottom).

420 **1.2.3 Estimate of Energy Loss before the TPC**

421 **1.3 Tracking Studies**

422 **1.3.1 Study of WC to TPC Match**

423 **1.4 Energy Calibration and Studies**

## 424 Chapter 2

# 425 Negative Pion Cross Section 426 Measurement

### 427 2.1 Raw Cross Section

### 428 2.2 Background Subtracted Cross Section

### 429 2.3 Efficiency Corrected Cross Section

## 430 Chapter 3

# 431 Positive Kaon Cross Section 432 Measurement

### 433 3.1 Raw Cross Section



# Appendix A

## Measurement of LArIAT Electric Field

The electric field of a LArTPC in the drift volume is a fundamental quantity for the proper functionality of this technology, as it affects almost every reconstructed quantity such as the position of hits or their collected charge. Given its importance, we calculate the electric field for LArIAT with a single line diagram from our HV circuit and we cross check the obtained value with a measurement relying only on TPC data.

Before getting into the details of the measurement procedures, it is important to explicit the relationship between some quantities in play. The electric field and the drift velocity ( $v_{drift}$ ) are related as follows

$$v_{drift} = \mu(E_{field}, T)E_{field}, \quad (\text{A.1})$$

where  $\mu$  is the electron mobility, which depends on the electric field and on the temperature (T). The empirical formula for this dependency is described in [?] and shown in Figure A.1 for several argon temperatures.

The relationship between the drift time ( $t_{drift}$ ) and the drift velocity is trivially

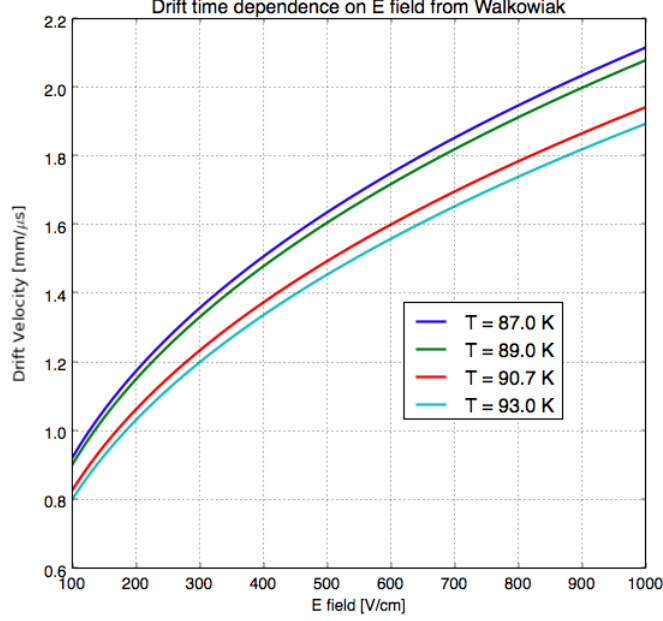


Figure A.1: Drift velocity dependence on electric field for several temperatures. The slope of the line at any one point represents the electron mobility for that given temperature and electric field.

Table A.1: Electric field and drift velocities in LArIAT smaller drift volumes

	Shield-Induction	Induction-Collection
$E_{field}$	700.63 V/cm	892.5 V/cm
$v_{drift}$	1.73 mm/ $\mu$ s	1.90 mm/ $\mu$ s
$t_{drift}$	2.31 $\mu$ s	2.11 $\mu$ s

450 given by

$$t_{drift} = \Delta x / v_{drift}, \quad (\text{A.2})$$

451 where  $\Delta x$  is the distance between the edges of the drift region. Table A.1 reports the  
452 values of the electric field, drift velocity, and drift times for the smaller drift volumes.

453 With these basic parameters established, we can now move on to calculating the  
454 electric field in the main drift region (between the cathode and the shield plane).

## Single line diagram method

The electric field strength in the LArIAT main drift volume can be determined knowing the voltage applied to the cathode, the voltage applied at the shield plane, and the distance between them. We assume the distance between the cathode and the shield plane to be 470 mm and any length contraction due to the liquid argon is negligibly small ( $\sim 2$  mm).

The voltage applied to the cathode can be calculated using Ohm's law and the single line diagram shown in Figure A.2. A set of two of filter pots for emergency power dissipation are positioned between the Glassman power supply and the cathode, one at each end of the feeder cable, each with an internal resistance of  $40\text{ M}\Omega$ .

Given the TPC resistor chain, the total TPC impedance is  $6\text{ G}\Omega$ . Since the total resistance on the circuit is driven by the TPC impedance, we expect the resulting current to be

$$I = V_{PS}/R_{tot} = -23.5\text{ kV}/6\text{ G}\Omega \sim 4\text{ }\mu\text{A}, \quad (\text{A.3})$$

which we measure with the Glassman power supply, shown in Figure A.3.

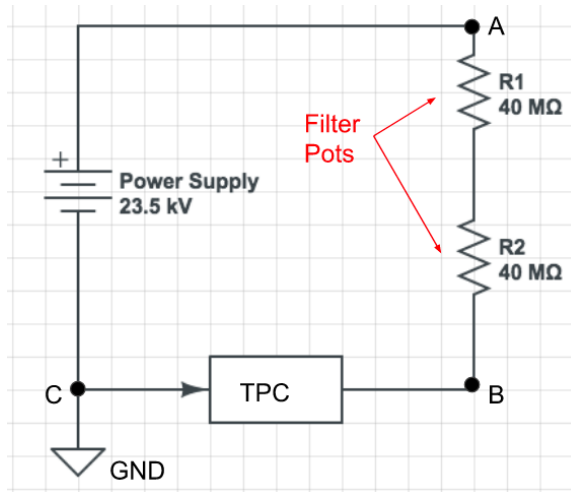


Figure A.2: LArIAT HV simple schematics.

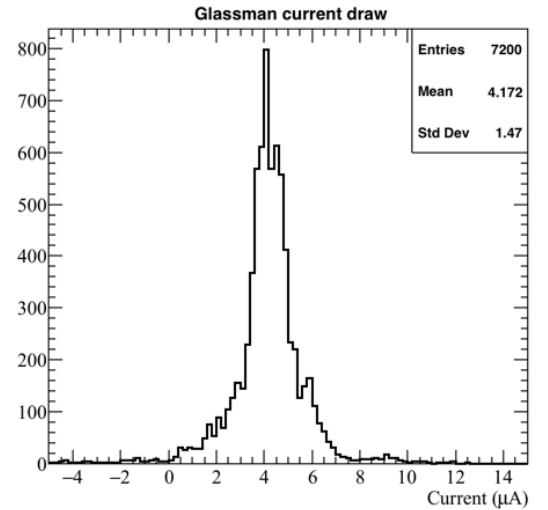


Figure A.3: Current reading from the Glassman between May 25th and May 30th, 2016 (typical Run-II conditions).

469 Using this current, the voltage at the cathode is calculated as

$$V_{BC} = V_{PS} - (I \times R_{eq}) = -23.5 \text{ kV} + (0.00417 \text{ mA} \times 80 \text{ M}\Omega) = -23.17 \text{ kV}, \quad (\text{A.4})$$

470 where  $I$  is the current and  $R_{eq}$  is the equivalent resistor representing the two filter  
471 pots. The electric field is then calculated to be

$$E_{\text{field}} = \frac{V_{BC} - V_{\text{shield}}}{\Delta x} = 486.54 \text{ V/cm}. \quad (\text{A.5})$$

## 472 **E field using cathode-anode piercing tracks**

473 We devise an independent method to measure the drift time (and consequently drift  
474 velocity and electric field) using TPC cathode to anode piercing tracks. We use this  
475 method as a cross check to the single line method. The basic idea is simple:

- 476 0. Select cosmic ray events with only 1 reconstructed track
- 477 1. Reduce the events to the one containing tracks that cross both anode and cath-  
478 ode
- 479 2. Identify the first and last hit of the track
- 480 3. Measure the time difference between these two hits ( $\Delta t$ ).

481 This method works under the assumptions that the time it takes for a cosmic particle  
482 to cross the chamber ( $\sim \text{ns}$ ) is small compared to the charge drift time ( $\sim \text{hundreds}$   
483 of  $\mu\text{s}$ ).

484 We choose cosmic events to allow for a high number of anode to cathode piercing  
485 tracks (ACP tracks), rejecting beam events where the particles travel almost perpen-  
486 dicularly to drift direction. We select events with only one reconstructed track to  
487 maximize the chance of selecting a single crossing muon (no-michel electron). We  
488 utilize ACP tracks because their hits span the full drift length of the TPC, see figure

489 A.4, allowing us to define where the first and last hit of the tracks are located in space  
490 regardless of our assumption of the electric field.

491 One of the main features of this method is that it doesn't rely on the measurement  
492 of the trigger time. Since  $\Delta t$  is the time difference between the first and last hit of a  
493 track and we assume the charge started drifting at the same time for both hits, the  
494 measurement of the absolute beginning of drift time  $t_0$  is unnecessary. We boost the  
495 presence of ACP tracks in the cosmic sample by imposing the following requirements  
496 on tracks:

- 497 • vertical position (Y) of first and last hits within  $\pm 18$  cm from TPC center  
498 (avoid Top-Bottom tracks)
- 499 • horizontal position (Z) of first and last hits within 2 and 86 cm from TPC front  
500 face (avoid through going tracks)
- 501 • track length greater than 48 cm (more likely to be crossing)
- 502 • angle from the drift direction (phi in figure A.5) smaller than 50 deg (more  
503 reliable tracking)
- 504 • angle from the beam direction (theta in figure A.5) greater than 50 deg (more  
505 reliable tracking)

506 Tracks passing all these selection requirements are used for the  $\Delta t$  calculation.

507 For each track passing our selection, we loop through the associated hits to retrieve  
508 the timing information. The analysis is performed separately on hits on the collection  
509 plane and induction plane, but lead to consistent results. As an example of the time  
510 difference, figures A.6 and A.7 represent the difference in time between the last and  
511 first hit of the selected tracks for Run-II Positive Polarity sample on the collection  
512 and induction plane respectively. We fit with a Gaussian to the peak of the  $\Delta t$   
513 distributions to extract the mean drift time and the uncertainty associated with it.

514 The long tail at low  $\Delta t$  represents contamination of non-ACP tracks in the track  
 515 selection. We apply the same procedure to Run-I and Run-II, positive and negative  
 516 polarity alike.

517 To convert  $\Delta t$  recorded for the hits on the induction plane to the drift time we  
 518 employ the formula

$$t_{drift} = \Delta t - t_{S-I} \quad (\text{A.6})$$

519 where  $t_{drift}$  is the time the charge takes to drift in the main volume between the  
 520 cathode and the shield plane and  $t_{S-I}$  is the time it takes for the charge to drift from  
 521 the shield plane to the induction plane. In Table A.1 we calculated the drift velocity  
 522 in the S-I region, thus we can calculate  $t_{S-I}$  as

$$t_{S-I} = \frac{l_{S-I}}{v_{S-I}} = \frac{4mm}{1.73mm/\mu s} \quad (\text{A.7})$$

523 where  $l_{S-I}$  is the distance between the shield and induction plane and  $v_{S-I}$  is the drift  
 524 velocity in the same region. A completely analogous procedure is followed for the hits  
 525 on the collection plane, taking into account the time the charge spent in drifting from  
 526 shield to induction as well as between the induction and collection plane. The value  
 527 for  $\Delta t_{drift}$ , the calculated drift velocity ( $v_{drift}$ ), and corresponding drift electric field  
 528 for the various run periods is given in Table A.2 and are consistent with the electric  
 529 field value calculated with the single line diagram method.

**Delta  $t_{drift}$ , drift  $v$  and E field with ACP tracks**

Data Period	$\Delta t_{Drift} [\mu s]$	Drift velocity $[mm/\mu s]$	E field $[V/cm]$
RunI Positive Polarity Induction	$311.1 \pm 2.4$	$1.51 \pm 0.01$	$486.6 \pm 21$
RunI Positive Polarity Collection	$310.9 \pm 2.6$	$1.51 \pm 0.01$	$487.2 \pm 21$
RunII Positive Polarity Induction	$315.7 \pm 2.8$	$1.49 \pm 0.01$	$467.9 \pm 21$
RunII Positive Polarity Collection	$315.7 \pm 2.7$	$1.49 \pm 0.01$	$467.9 \pm 21$
RunII Negative Polarity Induction	$315.9 \pm 2.6$	$1.49 \pm 0.01$	$467.1 \pm 21$
RunII Negative Polarity Collection	$315.1 \pm 2.8$	$1.49 \pm 0.01$	$470.3 \pm 21$
Average Values	314.1	$1.50 \pm 0.01$	$474.3 \pm 21$

Table A.2:  $\Delta t$  for the different data samples used for the Anode-Cathode Piercing tracks study.

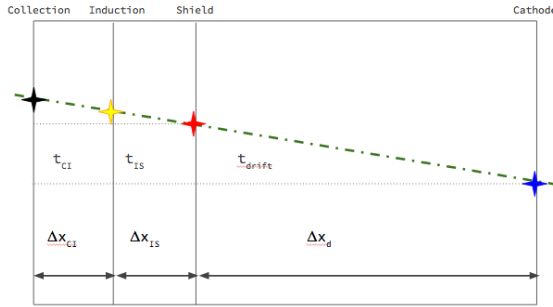


Figure A.4: Pictorial representation of the YX view of the TPC. The distance within the anode planes and between the shield plane and the cathode is purposely out of proportion to illustrate the time difference between hits on collection and induction. An ACP track is shown as an example.

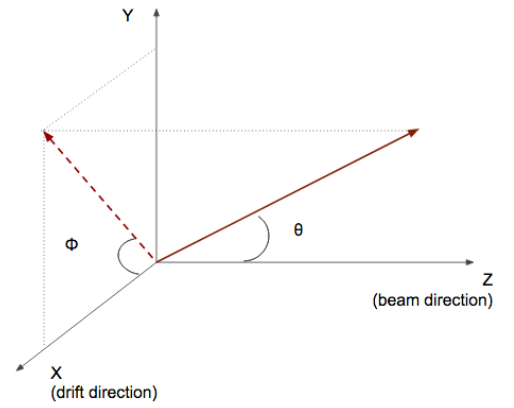


Figure A.5: Angle definition in the context of LArIAT coordinate system.

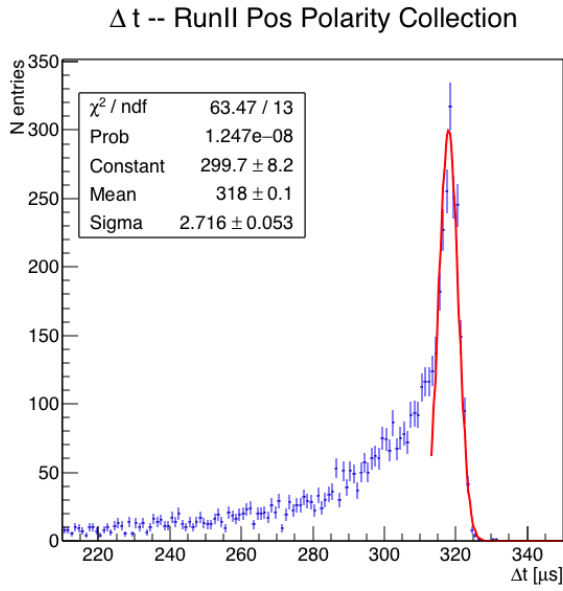


Figure A.6: Collection plane  $\Delta t$  fit for Run II positive polarity ACP data selected tracks.

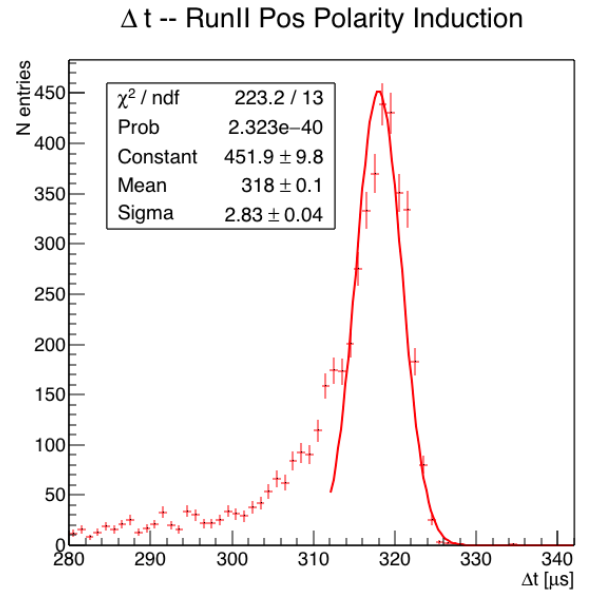


Figure A.7: Induction plane  $\Delta t$  fit for Run II positive polarity ACP data selected tracks.